EPJ manuscript No.
(will be inserted by the editor)

Continuum Random Phase Approximation with finite-range interactions

Giampaolo Co'[1] and Viviana De Donno[2] and Marta Anguiano[3] and Antonio M. Lallena[3]

[1] Dipartimento di Fisica "E. De Giorgi" Università del Salento, Lecce (Italy) and INFN sez. di Lecce (Italy),
[2] Dipartimento di Fisica "E. De Giorgi" Università del Salento, Lecce (Italy)
[3] Departamento de Física Atómica, Molecular y Nuclear, Universidad de Granada, E-18071 Granada, Spain

Received: date / Revised version: date

Abstract We rewrite the Random Phase Approximation secular equations in a form which allows the treatment of the continuum part of the single particle spectrum without approximations. Within this formalism finite-range interactions can be used without restrictions. We present some results, obtained with Gogny interactions, where the role of the continuum is relevant.

PACS. PACS-key describing text of that key – PACS-key describing text of that key

1 Introduction

The description of the nuclear response at energies above the particle emission threshold should consider a continuos excitation spectrum. Usually, the theories describing the nuclear excitations are based on mean-field models where the continuous part of the single particle (s.p.) spectrum is artificially discretized by imposing bound boundary conditions to all the s.p. wave functions. The use of discrete s.p. bases simplifies the description of the nuclear excited states, but it misses all the physics related to the emission of nucleons. Even in the investigation of the global properties of the excitations, the so-called escape width, which is not considered in discrete models, should be considered, since it is important for the proper description of giant resonances, especially in light and medium nuclei.

One of the theoretical approaches widely used to describe nuclear excitations is the Random Phase Approximation (RPA). The most common formulation of this theory is done by considering a discrete s.p. basis [1]. We shall call Discrete RPA (DRPA) this type of approach.

The limits of the DRPA have been overcome already since the beginning of the '70s. There are various approaches which solve the RPA equations by treating the continuum. They use Green's function [2,3,4,5,6,7], coordinate representation [8], coupled channel [9] or Fourier-Bessel [10] formulations. All these treatments heavily exploit the use of zero-range interactions to avoid the explicit evaluation of exchange matrix elements. Even the application of the RPA in infinite systems is based on this approximation, and the name RPA is used to indicate the sum of all the ring diagrams only [11].

Based on the work of Ref. [12], we propose here an RPA formalism which treats the continuum without approximations. This Continuum RPA (CRPA) approach can be applied to the use of finite-range interactions, since both direct and exchange matrix elements are explicitly calculated. To the best of our knowledge, our calculations are the first ones describing the nuclear ground state with the Hartree-Fock (HF) method and the excited states with the CRPA formalism, by using, in both type of calculations, the same finite-range interaction.

In the first part of this contribution, we present the main steps leading to the new formulation of the secular RPA equations which allows the treatment of the continuum. A more detailed derivation of the CRPA equations can be found in Refs. [13,14,15]. Some selected results which point out the need of properly treating the continuum are presented in the second part of the paper.

2 The model

The starting point of every many-body theory is the definition of the s.p. configuration space. In our approach we build this space by solving the Hartree-Fock equations

$$\mathcal{H}\left[\phi_k(\mathbf{r})\right] = -\frac{\hbar^2}{2m}\nabla^2\phi_k(\mathbf{r}) + \mathcal{U}(\mathbf{r})\,\phi_k(\mathbf{r}) - \int \mathrm{d}^3r'\,\mathcal{W}(\mathbf{r},\mathbf{r}')\,\phi_k(\mathbf{r}') = \epsilon_k\,\phi_k(\mathbf{r})\,, \tag{1}$$

where we have indicated with k the set of quantum numbers identifying the s.p. state. Since we deal with spherical nuclei only, these quantum numbers are the principal quantum number n, the orbital angular momentum l, the total angular momentum j, its projection on the quantization axis m, and the third component of the isospin t.

In Eq. (1) we have named the s.p. energy and wave function as ϵ_k and ϕ_k, respectively, and we have defined the Hartree,

$$\mathcal{U}(\mathbf{r}) \,=\, \sum_{\alpha=1}^{8} \sum_{k\leq \mathrm{F}} \int \mathrm{d}^3r' \, \phi_k^*(\mathbf{r}') \, V_\alpha(\mathbf{r},\mathbf{r}') \, \phi_k(\mathbf{r}') \,,$$

and the Fock-Dirac potentials

$$\mathcal{W}(\mathbf{r},\mathbf{r}') \,=\, \sum_{\alpha=1}^{8} \sum_{k\leq \mathrm{F}} \phi_k^*(\mathbf{r}') \, V_\alpha(\mathbf{r},\mathbf{r}') \, \phi_k(\mathbf{r}) \,,$$

where the sums are limited to those s.p. states with energies smaller than the Fermi energy.

We use finite-range interactions of the type

$$V_\alpha(\mathbf{r},\mathbf{r}') \,=\, v_\alpha(|\mathbf{r}-\mathbf{r}'|)\, O^\alpha \,, \;\; \alpha = 1,2,\ldots,8 \,,$$

where the various channels considered are

$$O^\alpha : 1 \,,\, \boldsymbol{\tau}\cdot\boldsymbol{\tau}' \,,\, \boldsymbol{\sigma}\cdot\boldsymbol{\sigma}' \,,\, \boldsymbol{\sigma}\cdot\boldsymbol{\sigma}'\,\boldsymbol{\tau}\cdot\boldsymbol{\tau}' \,,\, S(\mathbf{r},\mathbf{r}') \,,\, S(\mathbf{r},\mathbf{r}')\,\boldsymbol{\tau}\cdot\boldsymbol{\tau}'$$
$$(\mathbf{l}-\mathbf{l}')\cdot(\boldsymbol{\sigma}-\boldsymbol{\sigma}') \,,\, (\mathbf{l}-\mathbf{l}')\cdot(\boldsymbol{\sigma}-\boldsymbol{\sigma}')\,\boldsymbol{\tau}\cdot\boldsymbol{\tau}' \,,$$

In the above equation the symbols $\boldsymbol{\sigma}$, $\boldsymbol{\tau}$, S, $\mathbf{l}\,\boldsymbol{\sigma}'$, $\boldsymbol{\tau}'$, S' and $\mathbf{l}'$ indicate, respectively, the spin, isospin, tensor and orbital angular momentum operators of the two interacting particles.

The Gogny interaction [16,17], which we have used in our calculations, considers finite range functions v_α for all the channels up to α=6, and in the scalar, O^1, and isospin, O^2, terms it includes a dependence on the density of the system. Furthermore, it contains a spin-orbit term, O^7, of zero-range type and does not include the last channel, O^8. In the original parameterizations the tensor terms, $O^{5,6}$, were not considered. We have developed new parameterizations containing these terms and a discussion related to them is done in another contribution of this conference [18]. In the present article we shall consider only results obtained by using parameterizations without tensor terms.

Since we study spherical nuclei, we found convenient to express the s.p. wave functions as a product of a radial part and an angular momentum and spin dependent term

$$\phi_k^t(\mathbf{r}) \,=\, \phi_{nljm}^t(\mathbf{r}) \,=\, R_{nlj}^t(r)\, Y_{l,j}^m(\Omega) \,,$$

where $Y_{l,j}^m$ is the spin-spherical harmonics [19]. We recall that with k we indicate all the quantum numbers but the s.p. energy. The s.p. wave functions we consider are bound if ϵ_k is smaller than zero, while they have oscillatory asymptotic behavior in the other case, *i.e.* when they are in the continuum part of the energy spectrum. The radial part of these s.p. wave functions satisfies the closure relation

$$\sum_{\epsilon_k\leq\epsilon_\mathrm{F}} R_k(r,\epsilon_k)\, R_k^*(r',\epsilon_k) + \sum\!\!\!\!\!\!\int_{\epsilon_k>\epsilon_\mathrm{F}}^{\infty} R_k(r,\epsilon_k)\, R_k^*(r',\epsilon_k) \,=\, \delta(r-r') \,,$$

where the symbol in the second term indicates the sum on the bound levels above the Fermi energy and the energy integral of the s.p. continuos states. The sums and integrals must be done for a fixed set of quantum numbers $k \equiv (n,l,j,m,t)$.

The presence of s.p. states in the continuum requires to make explicit the dependence on the s.p. energy of the particle, ϵ_p, in the expression of the RPA operator

$$Q_\nu^\dagger \,=\, \sum_{ph} \sum\!\!\!\!\!\!\int_{\epsilon_p} \Big[X_{ph}^\nu(\epsilon_p)\, a_p^\dagger(\epsilon_p)\, a_h \,-\, Y_{ph}^\nu(\epsilon_p)\, a_h^\dagger\, a_p(\epsilon_p) \Big] \,,$$

here the subscript p, for particle, indicates all the quantum numbers characterizing a particle state with the exclusion of the energy ϵ_p, while the subscript h, for hole, considers also the s.p. energy ϵ_h. The RPA operator applied to the RPA ground state $|0\rangle$ generates the excited state $|\nu\rangle$ characterized by the total angular momentum J, parity Π and excitation energy ω

$$|\nu\rangle \equiv |J,\Pi,\omega\rangle = Q_\nu^\dagger\,|0\rangle \,.$$

By using traditional techniques [1] it is possible to obtain the RPA secular equations

$$(\epsilon_p - \epsilon_h - \omega)\, X_{ph}^\nu(\epsilon_p) + \sum_{p'h'} \sum\!\!\!\!\!\!\int_{\epsilon_{p'}} \Big[v_{ph,p'h'}^J(\epsilon_p,\epsilon_{p'})\, X_{p'h'}^\nu(\epsilon_{p'}) + u_{ph,p'h'}^J(\epsilon_p,\epsilon_{p'})\, Y_{p'h'}^\nu(\epsilon_{p'}) \Big] \,=\, 0 \,, \tag{2}$$

$$(\epsilon_p - \epsilon_h + \omega)\, Y_{ph}^\nu(\epsilon_p) + \sum_{p'h'} \sum\!\!\!\!\!\!\int_{\epsilon_{p'}} \Big[v_{ph,p'h'}^{J*}(\epsilon_p,\epsilon_{p'})\, Y_{p'h'}^\nu(\epsilon_p) + u_{ph,p'h'}^{J*}(\epsilon_p,\epsilon_{p'})\, X_{p'h'}^\nu(\epsilon_{p'}) \Big] \,=\, 0 \,. \tag{3}$$

In the DRPA equations, the X and Y amplitudes, and the interaction matrix elements u and v, do not depend explicitly on ϵ_p. In that case, the RPA secular equations are a homogeneous system of linear equations whose dimension is given by the number of particle-hole (ph) pairs. To be precise the dimension of the system is two times the ph number, because we have two unknowns, X and Y.

The CRPA equations depend on the continuous variable ϵ_p, therefore, the above expressions represent an infinite set of equations and it is necessary to rewrite these equations on a different form suitable to be solved. For this reason, we define two new functions:

$$f_{ph}^\nu(r) \,=\, \sum\!\!\!\!\!\!\int_{\epsilon_p} X_{ph}^\nu(\epsilon_p)\, R_p(r,\epsilon_p) \,,$$

$$g_{ph}^\nu(r) \,=\, \sum\!\!\!\!\!\!\int_{\epsilon_p} Y_{ph}^{\nu*}(\epsilon_p)\, R_p(r,\epsilon_p) \,.$$

In order to express the secular equations in terms of the new variables we multiply them by $R_p(r,\epsilon_p)$. For example

the first term of Eq. (2) becomes

$$(\epsilon_p - \epsilon_h - \omega)\, R_p(r,\epsilon_p)\, X^\nu_{ph}(\epsilon_p) \; = \; \mathcal{H}\,\left[R_p(r,\epsilon_p)\, X^\nu_{ph}(\epsilon_p)\right] - (\epsilon_h + \omega)\, R_p(r,\epsilon_p)\, X^\nu_{ph}(\epsilon_p)\,,$$

where we have used Eq. (1). By summing and integrating on ϵ_p we obtain

$$\sum\!\!\!\!\!\!\int_{\epsilon_p} \mathcal{H}\,\left[R_p(r,\epsilon_p)\, X^\nu_{ph}(\epsilon_p)\right] \; = \; \mathcal{H}\,\left[f^\nu_{ph}(r)\right]\,.$$

By applying these operations to all the terms of the secular equations we obtain

$$\mathcal{H}\left[f_{ph}(r)\right] \, - \, (\epsilon_h \, + \, \omega)\, f_{ph}(r) = - \, \mathcal{F}^J_{ph}(r) + \sum_{\epsilon_i<\epsilon_{\rm F}} \delta_{ip}\, R_i(r) \int {\rm d}r_1\, r_1^2\, R^*_i(r_1)\, \mathcal{F}^J_{ph}(r_1)\,, \tag{4}$$

$$\mathcal{H}\left[g_{ph}(r)\right] \, - (\epsilon_h \, - \, \omega)\, g_{ph}(r) = - \, \mathcal{G}^J_{ph}(r) + \sum_{\epsilon_i<\epsilon_{\rm F}} \delta_{ip}\, R_i(r) \int {\rm d}r_1\, r_1^2\, R^*_i(r_1)\, \mathcal{G}^J_{ph}(r_1)\,, \tag{5}$$

where we have defined

$$\begin{aligned}\mathcal{F}^J_{ph}(r) = \sum_{p'h'} \int {\rm d}r_2\, r_2^2 \; & \Big\{ R^*_{h'}(r_2) \, \Big[V^{J,{\rm dir}}_{ph,p'h'}(r,r_2)\, R_h(r)\, f_{p'h'}(r_2) \\ & - V^{J,{\rm exc}}_{ph,p'h'}(r,r_2) f_{p'h'}(r)\, R_h(r_2) \Big] \\ & + g^*_{p'h'}(r_2) \, \Big[U^{J,{\rm dir}}_{ph,p'h'}(r,r_2)\, R_h(r)\, R_{h'}(r_2) \\ & - U^{J,{\rm exc}}_{ph,p'h'}(r,r_2)\, R_{h'}(r)\, R_h(r_2) \Big] \Big\}\,.\end{aligned}$$

The term $\mathcal{G}^J_{ph}$ is obtained from the above equation by interchanging the f and g functions.

By using the procedure outlined above, we rewrote the original algebraic RPA secular equations as a finite set of integro-differential equations with unknowns depending on r. The solution of these equations requires the choice of appropriate boundary conditions. The physical process described by the CRPA secular equations is a many-body scattering process where a particle is emitted in the continuum. For a given value of the excitation energy ω, only those nucleons whose s.p. energy satisfies $|\epsilon_k| \le \omega$ can be emitted. The set of ph pairs where a particle can be emitted in the continuum is the set of the *open channels*. We solve the CRPA secular equations by imposing that the particle is emitted one at the time in a specific ph open channel which we specify as p_0h_0 and call *elastic channel*. From the mathematical point of view we solve Eqs. (4) and (5) by imposing the following boundary conditions for each open channel. For the f_{ph} function we have

$$f^{p_0h_0}_{ph}(r) \underset{r\to\infty}{\longrightarrow} R_{p_0}(r,\epsilon_{p_0})\, \delta_{p,p_0}\, \delta_{h,h_0} \, + \, \lambda\, H^-_p(\epsilon_h + \omega, r)\,,$$

with $\epsilon_{p_0} = \omega + \epsilon_{h_0}$. Here λ is a complex normalization constant, and $H^-_p(\epsilon_h+\omega,r)$ is the incoming Coulomb function for protons, and a Hankel function for neutrons. The boundary condition for g_{ph}, which is related to the contribution of correlations in the RPA ground state, is

$$g^{p_0h_0}_{ph}(r) \underset{r\to\infty}{\longrightarrow} \frac{1}{r}\, \exp\left[-r\left(\frac{2m|\epsilon_h-\omega|}{\hbar^2}\right)^{\frac{1}{2}}\right]\,.$$

From the physics point of view the problem is now well defined, but the solution of the CRPA secular equations (4) and (5) is rather involved. We solved this problem by carrying out an expansion of the f_{ph} and g_{ph} functions on a basis of Sturm-Bessel functions. These functions are solutions of the following differential equation [20]

$$\left[-\frac{\hbar^2}{2m}\left(\frac{{\rm d}^2}{{\rm d}r^2} \, + \, \frac{1}{r}\,\frac{\rm d}{{\rm d}r} \, - \, \frac{l_p(l_p+1)}{r^2}\right) \, - \, \epsilon_p\right] \Phi^\mu_p(r) \; = \; = \, - \, \overline{U}^\mu_p(r)\, \Phi^\mu_p(r)\,,$$

where

$$\overline{U}^\mu_p(r) \; = \; \begin{cases} \beta^\mu_p + i\gamma^\mu_p\,, & \text{if } r \le a\,, \\ 0\,, & \text{if } r > a\,, \end{cases}$$

and β and γ are real constants. In our calculations the values of a have been chosen to be the maximum values of the numerical integration box more than two times the nuclear radius. The Sturm-Bessel functions satisfy the orthogonality relation

$$(\beta^\mu_p + i\gamma^\mu_p) \int_0^a {\rm d}r\, r^2\, \Phi^\mu_p(r)\, \Phi^\nu_p(r) \; = \; \delta_{\mu\nu}\,.$$

Since the Sturm-Bessel functions are not, in general, orthogonal to the hole s.p. states, we found more convenient to use modifed Sturm-Bessel functions defined as

$$\widetilde{\Phi}^\mu_p(r) \; = \; \Phi^\mu_p(r) \, - \, \sum_{\epsilon_k<\epsilon_{\rm F}} \delta_{kp}\, R^*_k(r) \int {\rm d}r'\, r'^2\, R_k(r')\, \Phi^\mu_p(r')\,.$$

where the Kroneker's δ indicates that the quantum numbers identifying the hole s.p. state R_k must be the same as those of the particle state p.

Using these functions we write the f_{ph} and g_{ph} unknowns as

$$f^{p_0h_0}_{ph}(r) = R_{p_0}(r,\epsilon_{p_0})\, \delta_{pp_0}\, \delta_{hh_0} \, + \, \sum_\mu c^{\mu+}_{ph}\, \widetilde{\Phi}^{\mu+}_p(r)\,,$$

$$g^{p_0h_0}_{ph}(r) = \sum_\mu c^{\mu-}_{ph}\, \widetilde{\Phi}^{\mu-}_p(r)\,,$$

where the superscripts $+$ and $-$ indicate that the Sturm-Bessel functions are calculated at energies $\epsilon_p = \epsilon_h + \omega$ and $\epsilon_p = \epsilon_h - \omega$, respectively.

By inserting the above expressions in the CRPA secular equations (4) and (5), and exploiting the orthogonality properties of the modified Sturm-Bessel functions we obtain a set of algebraic equations whose unknowns are the expansion coefficients $c^{\mu\pm}_{ph}$. The explicit expression of these equations is given in Refs. [13,14,15]. From the numerical

point of view the limitation of this approach is related to the truncation of the number of expansion coefficients of the f_{ph} and g_{ph} functions. We have verified that already 5 or 6 expansion coefficients provide convergence of the results of the responses at the third significant digit. In all the calculations we used 10 expansion coefficients.

The knowledge of the f_{ph} and g_{ph} allows a straightforward evaluation of observables. We consider, at the moment, observables which can be described by one-body operators as

$$T_{JM}(\mathbf{r}) = \sum_{i=1}^{A} F_J(r_i)\,\theta_{JM}(\Omega_i)\,\delta(\mathbf{r}_i - \mathbf{r}) \ ,$$

where r and Ω indicate, respectively, the radial and angular components of the spherical polar coordinates. For each elastic channel, we can write the transition amplitude related to this operator as:

$$\langle J\|T_J\|0\rangle_{p_0h_0} = \\ = \sum_{ph} \left[\langle j_p\|\theta_J\|j_h\rangle \int \mathrm{d}r\, r^2\, (f_{ph}^{p_0h_0}(r))^*\, F_J(r)\, R_h(r) \right. \\ \left. + (-1)^{J+j_p-j_h}\, \langle j_h\|\theta_J\|j_p\rangle \int \mathrm{d}r\, r^2\, R_h^*(r)\, F_J(r)\, g_{ph}^{p_0h_0}(r) \right] .$$

The observables we have considered are obtained by carrying out incoherent sums on all the elastic channels of the square of the transition amplitudes

$$\sigma \sim \sum_{p_0h_0} |\langle J\|T_J\|0\rangle_{p_0h_0}|^2 \ .$$

3 Results

In this section, we discuss some selected results of our calculations with the aim of emphasizing the need of a detailed description of the continuum excitation.

A direct comparison between DRPA and CRPA results is presented in Fig. 1, where we show the contribution of the 1^- and 2^+ multipole excitations to the total photoabsorption cross section of the ^{16}O nucleus. The vertical lines indicate the DRPA results while the red dashed curves correspond to CRPA. These results have been obtained with two different parameterizations of the Gogny interaction: the D1S [16] and the D1M [17].

We observe that the positions of the main peaks of the DRPA correspond to those of the maxima of the CRPA responses. In particular, the DRPA results for the 1^- excitation indicate the presence of the giant resonance region. Obviously, the CRPA results shape much better the presence of this resonance. The main failure of the DRPA is in the region above the giant resonance where the DRPA peaks form cluster while the CRPA results have a smooth behavior. The clustering of the DRPA solutions is a factitious feature which does not have any physical meaning. The situation is even more evident in the excitation of the 2^+ mode.

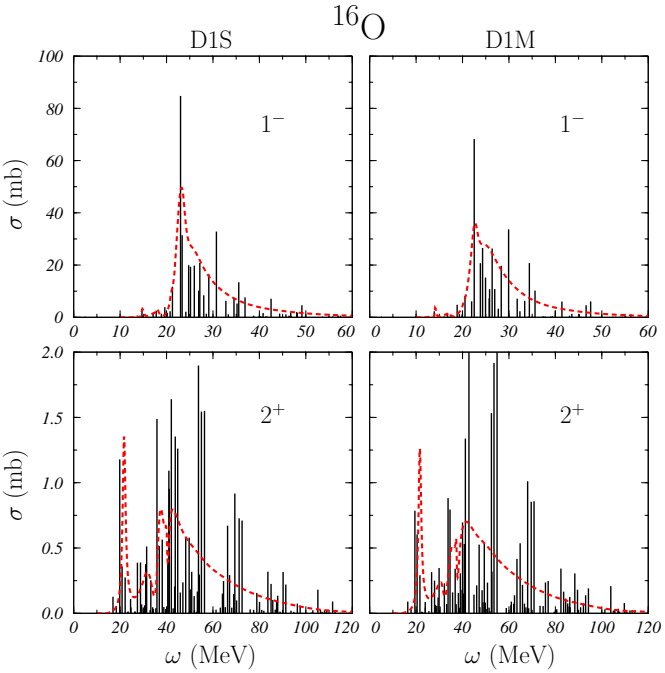

Figure 1. (Color on line) Contribution of the 1^- and 2^+ multipole excitations to the total photoabsorption cross section in ^{16}O. The vertical lines and red dashed curves show, respectively, the DRPA and CRPA results obtained with two different parameterisations of the Gogny interaction.

The integrated DRPA and CRPA strengths, obtained with the same interaction, coincide within the numerical accuracy. This indicates that by properly treating the continuum we do not produce additional strength, but we smooth the global strength by considering that the (continuum) particle wave functions have an escape energy width. The contribution of the 2^+ strength to the total photoabsorption cross section is one order of magnitude smaller than that of the 1^-, as it is shown by the different scales on the y-axes of Fig. 1. The 2^+ strength is more spread than that of the 1^-. The value of the 1^- cross section at 60 MeV is about 2% of that at the maximum, around 23 MeV. The value of the 2^+ cross section at 60 MeV is half that of the maximum, at about 40 MeV. At excitation energies above 100 MeV we obtain values of few percent

In the panel (a) of Fig. 2 we compare the results of our calculations with the experimental data of Ref. [21]. The blue dashed and green solid curves have been obtained by using the D1M interaction; the red dashed-dotted and black dotted lines correspond to the D1S force. The green solid and black dotted curves show the Independent Particle Model (IPM) results that have been obtained by switching off the residual interaction in the CRPA calculations. It is evident that the presence of the collectivity induced by the residual interaction in the CRPA calculation generates the resonant behavior of the cross section. The position of the peak is rather well reproduced, especially by considering that these are parameter free calculations. The limits of the RPA theory become evident by

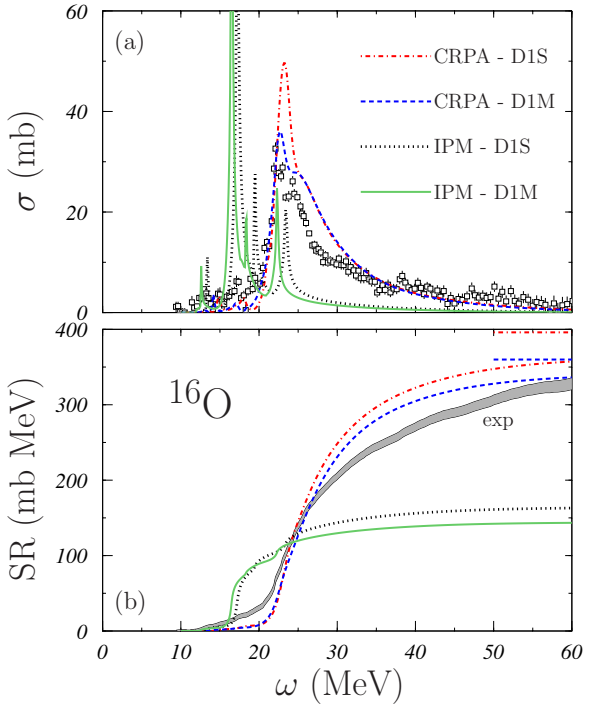

Figure 2. (Color on line) Panel (a): Total photoabsorption cross section experimental data [21] compared with the results of various calculations. The D1S and D1M labels indicate the force used in the CRPA and IPM calculations. Panel (b): Sum rule exhaustion function, as defined in Eq. (6), for the results shown in panel (a). The grey area indicates the results obtained by using the experimental data. The horizontal lines in the right upper corner show the expected asymptotic values in the CRPA calculations for the D1S and D1M forces.

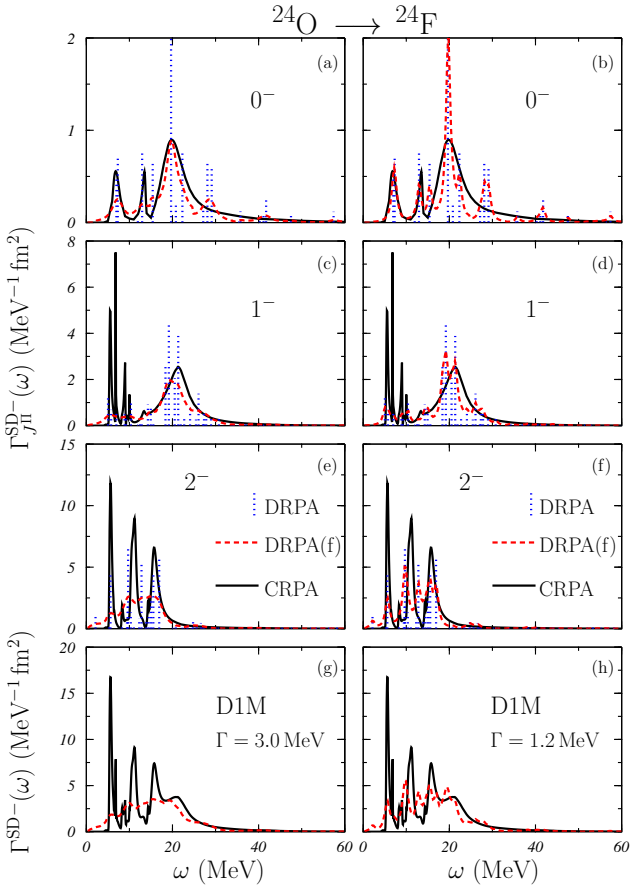

Figure 3. (Color on line) Neutron-proton spin dipole excitation strengths in ^{24}O. All the multipole excitations indicated in the labels contribute to the total strength which is obtained as sum of their contributions and it is shown in the (g) and (h) panels. The DRPA results are indicated by the blue dotted vertical linew while the CRPA results by the black full lines. The red dashed lines have been obtained by folding the DRPA results with Lorentz functions of widths 3.0 MeV (left panels) and 1.2 MeV (right panels).

observing that the experimental width is larger than the theoretical one. This can be appreciated by observing the behavior of the sum rule exhaustion functions calculated as

$$SR(\omega) = \int_0^\omega d\omega' \, \sigma(\omega') \, , \qquad (6)$$

and shown in the panel (b) of Fig. 2. At 60 MeV the sum rule value for the results obtained with the D1M force, almost coincides with the experimental one, while the sum rule value obtained with the D1S force is about 10% larger than the experimental value. This indicates that the major discrepancy with the experimental results is not due to the total strength but rather to its distribution which is too much concentrated in the resonance region between 20 and 40 MeV. The CRPA curves in panel (b) have a much steeper behavior than the experimental one, even though they reach almost the same values at 60 MeV. The source of this discrepancy is attributed to the fact that the RPA does not consider the so-called spreading width, which, in our formalism, would correspond to consider particle-hole excitations beyond one-particle one-hole. Discrete RPA calculations which include the spreading width improve the agreement with the experimental data. To the best of our knowledge there are not calculations which consider on the same ground continuum and spreading width.

The results of Fig. 2 could induce to consider that the effects of the continuum can be simulated by spreading the DRPA results with a Lorentz function which, by construction, conserves the total cross section.

The results of Fig. 3 point out the problems related to this procedure. In this figure, we show the charge-exchange excitation transforming ^{24}O in ^{24}F induced by the spin-dipole operator

$$T^{\mathrm{SD}\pm}_{J^-,M} = \sum_{i=1}^{A} r_i \, [Y_1(i) \otimes \boldsymbol{\sigma}(i)]^J_M \, t_\pm(i) \, , \qquad (7)$$

which can excite the 0^-, 1^- and 2^- multipoles. The total strength, which, in our case, is shown in the panels (g) and (h), is obtained by summing the strengths of each individual excitation.

The black full lines show the CRPA results. They are repeated in the left and right panels. The blue vertical dotted lines show the results of DRPA calculations, and they are also repeated in the left and right panels. Evidently, the DRPA solutions appear at discrete energies and this makes impossible their sum to obtain the global response. The usual procedure consists in folding the various DRPA responses with a Lorentz function which, by definition, conserves the integrated value of the strength. The DRPA responses we obtain after the folding are shown in the figure by the red dashed lines. The results of the left panels have been obtained by using a value of the Lorentz width of 3.0 MeV. This value has been chosen to reproduce the 0^- CRPA strength. The right panels show the results we obtain by using a Lorentz width value of 1.2 MeV which has been selected to reproduce the 2^- CRPA strength. None of the two choices produces satisfactory results. The global CRPA strength is not well reproduced since the good description of one of the multipole excitations makes worst the description of the other ones.

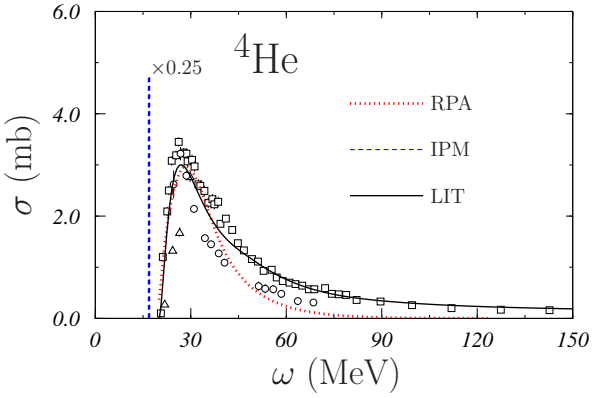

Figure 4. (Color on line) Total photoabsorption cross section in ^{4}He. The experimental data are taken from Refs. [22,23,24]. The red dotted line shows the CRPA result and the blue dashed line the IPM result. With the black full line we show the LIT results of Ref. [25].

Since the main limitation of our RPA approach is the lack of spreading width, we have applied our computational scheme to a system where it is negligible, the ^{4}He nucleus. The HF calculations do not provide a good description of the ground state. For the binding energy, we obtain 30.28 MeV and 29.54 MeV for the D1S and D1M forces respectively, to be compared with the experimental value of 28.29 MeV. The theoretical rms charge radii are 2.04 fm and 2.02 fm for the D1S and D1M respectively, against the experimental value of 1.68 fm.

Despite the poor description of the ground state properties our approach provides a reasonable description of the excitation of this system. We show in Fig. 4 the comparison of the results of our calculations with the experimental data [22,23,24] and with the results of the Lorentz Inverse Transform (LIT) method [25] obtained by using a microscopic nucleon-nucleon interaction. In the figure, the red dashed line shows the CRPA result which, in the peak region, compares rather well with the data and also with the LIT results (black solid curve). The discrepancy in the high energy tail could be due to phenomena such as the disintegration of ^{4}He in two deuterons, effects which are not included in the RPA which considers 1p-1h excitations only. Also, it is worth pointing out that our calculations do not consider tensor force and short-range correlations and they could also produce relevant effects in this kinematic region. In any case, the agreement with the data is certainly better than that of ^{16}O shown in Fig. 2. The IPM (blue dashed curve) fails badly in describing the presence of the resonance also in ^{4}He.

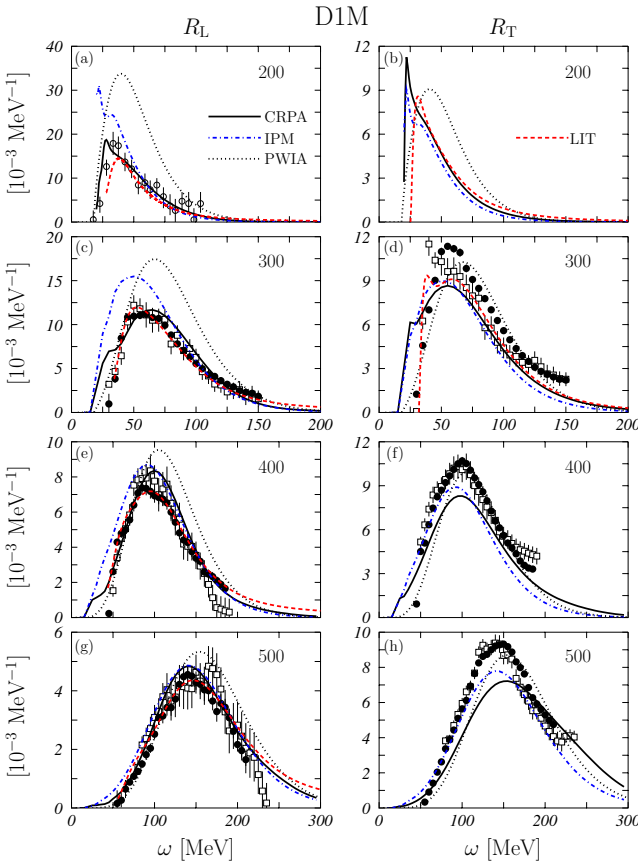

Figure 5. Electron scattering longitudinal, R_L, and transverse, R_T, responses for different values of the momentum transfer indicated in the labels of the various panels in MeV/c units. The experimental data are those of Refs. [27,28,29]. The black full lines show the CRPA results, the blue dashed-dotted correspond to the IPM calculations and the black dotted lines are the PWIA results. When available, we show with red dashed lines also the LIT results [30,31,32].

The calculation of the electron scattering responses requires the evaluation of many multipole excitations. We show in Fig. 5 the longitudinal, R_L, and transverse, R_T, responses for different values of the momentum transfer. The details of the calculation of the electron scattering responses are given in Ref. [26].

The experimental data of Refs. [27,28,29] and the results of LIT [30,31,32] are compared with various types of calculations. The black full lines indicate the CRPA results obtained with the D1M calculations. It is remarkable the agreement of our effective theory with the LIT theory which is based on microscopic interactions. The agreement with the data of the longitudinal response is very good. The transverse response data are, however, underestimated. This is the same situation we have encountered in heavier nuclei where we had to insert a phenomenological spreading width. Clearly in the case of ^{4}He the role of the spreading width is negligible.

The black dotted curves show results where we use a plane wave to describe the wave function of the emitted particle. We call these results as Plane Wave Impulse Approximation (PWIA). These responses are very different from those of the CRPA calculations. The blue dashed-dotted lines show the IPM responses. The difference between the IPM responses and those of the CRPA becomes smaller with increasing value of the momentum transfer. In a model which considers the RPA as sum of all the ring diagrams with a finite-range interaction for large value of the momentum transfer the interacting response is equal to the free one [33]. Even though the free and interacting responses are equal for large values of the momentum transfer, their difference is remarkable at lower values.

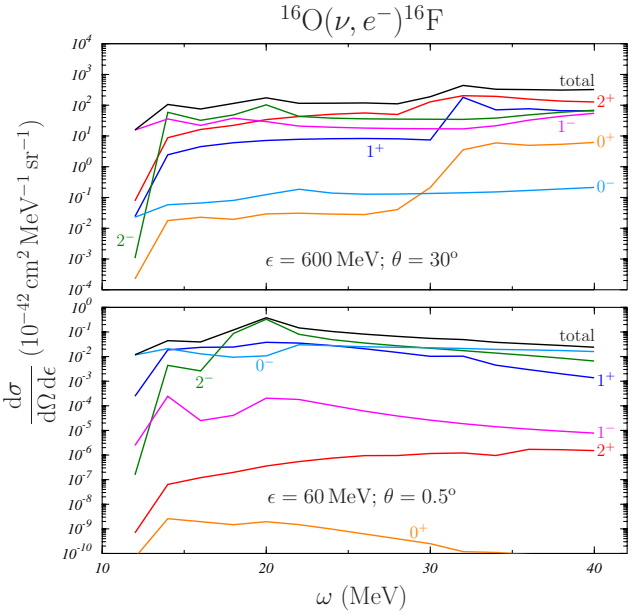

Figure 6. (Color on line) Charge exchange neutrino cross sections on ^{16}O nucleus for different values of the incoming energy ϵ and scattering angle θ. The various coloured lines indicate the contribution of each excitation multipole to the total cross section represented by the black line.

The potentiality of our approach can be seen in Fig.6 where we present the charge-exchange neutrino cross section on the ^{16}O nucleus, calculated as indicated in Ref. [34]. The two panels show the cross sections for two different kinematic conditions. The energy of the incoming neutrino ϵ is different and also the scattering angle θ. The color codes indicate the contribution of the different multipoles to the total cross sections which are represented by the black solid lines. The calculations have been carried out by using the CRPA wave functions obtained with the D1M interaction.

The relative contribution of the various multipoles considered changes deeply in the two cases. For example the 0^- cross section which is five order of magnitude smaller than the total cross section when $\epsilon = 600$ MeV, is a fundamental component of the cross section for $\epsilon = 60$ MeV where it becomes the most important component for excitation energies ω above 30 MeV.

4 Conclusions

In this contribution we have reformulated the CRPA secular equations by using new unknowns which are function of the nucleon coordinate. These equations form a set of integro-differential equations which we solve by using a technique based on an expansion on a Sturm-Bessel function basis.

The proper treatment of the continuum is necessary to describe nuclear excitations at the giant resonance energies and above. The commonly adopted technique of folding the DRPA solutions with Lorentz functions can produce errors when different multipole excitations must be considered.

The comparison with the photon and electron scattering cross sections in ^{4}He is remarkably good, much better than for the ^{16}O nucleus. This is related to the intrinsic limitation of the RPA which consider only 1p-1h excitation and, therefore, it neglects the so-called spreading width. The presence of the spreading width is negligible in ^{4}He, but relevant in heavier nuclei.

References

1. P. Ring, P. Schuck, The nuclear many-body problem, Springer, Berlin, 1980.
2. S. Shlomo, G. F. Bertsch, Nucl. Phys. A 243 (1975) 507.
3. N. van Giai, H. Sagawa, Nucl. Phys. A 371 (1981) 1.
4. N. Auerbach, A. Klein, Nucl. Phys. A 395 (1983) 77.
5. M. Waroquier, et al., Phys. Rep. 148 (1987) 249.
6. T. Nakatsukasa, K Yabana, Phys. Rev. C 71 (2005) 024301.
7. K. Mizuyama, G. Colò, E. Vigezzi, Phys. Rev. C 86 (2012) 034318.
8. I. Hamamoto, H. Sagawa, Phys. Rev. C 60 (1999) 064314.
9. A. M. Saruis, Phys. Rep. 235 (1993) 57.
10. R. de Haro, S. Krewald, J. Speth, Nucl. Phys. A 388 (1982) 265.
11. A. L. Fetter, J. D. Walecka, Quantum theory of many-particle systems, McGraw-Hill, S. Francisco, 1971.
12. M. Buballa, S. Drożdż, S. Krewald, J. Speth, Ann. of Phys. 208 (1991) 346.
13. V. De Donno, Nuclear excited states within the Random Phase Approximation theory, Ph.D. thesis, Università del Salento (Italy) (2008), http://www.fisica.unisalento.it/ gpco/stud.html.

14. V. De Donno, G. Co', M. Anguiano, A. M. Lallena, Phys. Rev. C 83 (2011) 044324.
15. V. De Donno, G. Co', M. Anguiano, A. M. Lallena, Self-consistent continuum Random Phase Approximation with finite-range interactions for charge-exchange excitations, submitted to Phys. Rev. C.
16. J.F. Berger, M. Girod and D. Gogny, Comp. Phys. Commun. 63, (1991) 365.
17. S. Goriely, S. Hilaire, M. Girod and S. Péru, Phys. Rev. Lett. 102, (2009) 242501.
18. M. Anguiano, A. M. Lallena, G. Co', V. De Donno, M. Grasso, R. N. Bernard, Gogny interactions with tensor terms, contribution to this volume.
19. A. R. Edmonds, Angular momentum in quantum mechanics, Princeton University Press, Princeton, 1957.
20. G. Rawitscher, Phys. Rev. C. 25 (1982) 2196.
21. J. Ahrens, et al., Nucl. Phys. A 251 (1975) 479.
22. Y. M. Arkatov, et al., Yad. Konst. 4 (1979) 55.
23. T. Shima, S. Naito, Y. Nagai, T. Baba, K. Tamura, T. Takahashi, T. Kii, H. Ohgaki, H. Toyokawa, Phys. Rev. C 72 (2005) 044004.
24. B. Nilsson, et al., Phys. Lett. B 626 (2005) 65.
25. D. Gazit, S. Bacca, N. Barnea, W. Leidemann, G. Orlandini, Phys. Rev. Lett. 96 (2006) 112301.
26. J. E. Amaro, G. Co', A. M. Lallena, Ann. Phys. (NY) 221 (1993) 306.
27. A. yu. Buki, I. S. Timchenko, N. G. Shevchenko, I. A. Nenko, Phys. Lett. B 641 (2006) 156.
28. K. F. von Reden, et al., Phys. Rev. C 41 (1990) 1084.
29. A. Zghiche, et. al, Nucl. Phys. A 572 (1994) 513.
30. S. Bacca, H. Arenhövel, N. Barnea, W. Leidemann, G. Orlandini, Phys. Rev. C 76 (2007) 014003.
31. S. Bacca, N. Barnea, W. Leidemann, G. Orlandini, Phys. Rev. Lett. 102 (2009) 162501.
32. S. Bacca, N. Barnea, W. Leidemann, G. Orlandini, Phys. Rev. C 80 (2009) 064001.
33. M. Martini, G. Co', M. Anguiano, A. M. Lallena, Phys. Rev. C 75 (2007) 034604.
34. A. Botrugno, G. Co' Nucl. Phys. A761 (2005) 200.